chemosensors

MDPI

Article

A Red-Emitting Fluorescence Probe for Rapid Detecting Exogenous and Endogenous Peroxynitrite in Living Cells with High Sensitivity and Selectivity

Bing Jin [1,*,†], Jing Liu [2,†], Longsheng Jin [1], Weishuai Liu [1] and Xiangjun Liu [2,*]

[1] Department of Chemistry, College of Sciences, Nanjing Agricultural University, 1 Weigang, Nanjing 210095, China; 2022211001@stu.njau.edu.cn (L.J.); 2021111022@stu.njau.edu.cn (W.L.)
[2] Beijing National Laboratory for Molecular Sciences, Key Laboratory of Analytical Chemistry for Living Biosystems, CAS Research/Education Center for Excellence in Molecular Sciences, Institute of Chemistry, Chinese Academy of Sciences, Beijing 100190, China; liujing231023@163.com
* Correspondence: jinbing@njau.edu.cn (B.J.); xjliu@iccas.ac.cn (X.L.)
† These authors contributed equally to this work.

Abstract: Peroxynitrite ($ONOO^-$) has been revealed to play crucial roles in many physiological and pathological processes, and many diseases were proven to be associated with its misregulated production. The development of fluorescent probes meets the need for tracking $ONOO^-$ and gives a better understanding of its diverse mechanisms. In this work, a red-emitting fluorescent probe BP-ONOO was synthesized via functionalization of the rhodol-like fluorophore with a reactive site of hydrazide. The probe BP-ONOO exhibited high sensitivity, excellent selectivity, and short response time (less than 4 s) towards $ONOO^-$ under neutral or weak alkaline conditions. These attractive properties favor its application in real-time imaging of $ONOO^-$ in living cells, and the probe has been successfully applied for imaging the concentration levels of $ONOO^-$ in RAW 264.7 macrophage cells under drug stimulation.

Keywords: peroxynitrite; fluorescent probe; red-emitting; exogenous and endogenous

Citation: Jin, B.; Liu, J.; Jin, L.; Liu, W.; Liu, X. A Red-Emitting Fluorescence Probe for Rapid Detecting Exogenous and Endogenous Peroxynitrite in Living Cells with High Sensitivity and Selectivity. *Chemosensors* **2023**, *11*, 555. https://doi.org/10.3390/chemosensors11110555

Academic Editor: Young-Tae Chang

Received: 8 October 2023
Revised: 18 October 2023
Accepted: 30 October 2023
Published: 6 November 2023

1. Introduction

Peroxynitrite ($ONOO^-$), one of the highly reactive nitrogen species (hRNS) in living systems, is generated via a rapid radical–radical coupling interaction between nitric oxide radicals (•NO) and superoxide anion radicals ($O_2^{\bullet -}$) [1]. Accumulating evidence suggests that $ONOO^-$ is highly prevalent in endothelial cells, macrophages, leukocytes, neutrophils, and nerve cells and plays a positive role in signal transduction and immunogenic response [2–4]. On the other hand, $ONOO^-$, possessing strong oxidability and nucleophilicity, is also considered to be cytotoxic because it can damage a magnitude of biomolecules and eventually cause cell necrosis or apoptosis [5,6]. Many diseases, including neurodegenerative, diabetes, cardiovascular diseases, and cancers, have been reported to be associated with the misregulated production of $ONOO^-$ in vivo [7–10]. Owing to its short half-life, low concentration, and high reactivity in living systems, it is still a challenge to fully understand the exact mechanisms and diverse roles of biological $ONOO^-$ [11]. Thus, researchers are pursuing an effective technology that can monitor the concentration variation of $ONOO^-$ in physiological and pathological processes with high sensitivity and selectivity [12].

The fluorescent probe technique is distinguished by its inherent advantages, including simplicity, fast response, high sensitivity/selectivity, and noninvasiveness. It is widely recognized as a valuable tool for providing information on biological events with exceptional spatio-temporal resolution [13]. Thus far, great effort has been made to develop probes for detecting $ONOO^-$ in the biosystems [12,13]. Due to the oxidizing/nucleophilic

nature of $ONOO^-$, a variety of functional groups, generally comprising boronates [14], α-ketoamides [15], hydrazides [16], diphenyl phosphinates [17], C=C bonds [18], trifluoroketones [19], and other active moieties [20–22], were added as triggers to fluorophores. However, some of them suffered from a lack of selectivity for $ONOO^-$ against other reactive oxygen species (ROS)/reactive nitrogen species (RNS). When high concentrations (micromolar range) of these reactive species coexist with $ONOO^-$ (nanomolar range), they may seriously interfere with $ONOO^-$ detection by reacting with triggers with a similar oxidation mechanism [23,24]. Meanwhile, fluorescent probes with emission spectra in the far-infrared to NIR regions have received great attention. Cheng et al. have screened a series of NIR fluorescent probes for imaging $ONOO^-$ to assess drug-induced hepatotoxicity [25], which features minimum phototoxicity to the biological samples, high imaging depth, and low auto-fluorescence interference from biomolecules. In view of the low concentration, the short half-life of $ONOO^-$, and the existence of a variety of strong interferences in biological systems, it is still necessary to engineer fast-response, long-wavelength fluorescent probes with improved sensitivity and selectivity.

Previous studies have indicated that incorporating a hydrazide group into rhodamine-type fluorophores to form spirolactam has been proved to be an effective strategy [16,26,27]. Probes designed using this approach can undergo a ring-opening process of Xanthene structures and exhibit an "off-on" signal change with the addition of $ONOO^-$ compared to other ROS/RNS. However, certain limitations exist in some of these probes regarding their selectivity, as they may also recognize ClO^- and •OH [28]. Therefore, we hypothesized that the selection of an appropriate fluorophore as well as recognition groups is critical. BP613 is a recently reported rhodol-like fluorophore [29] which possesses several desired properties, such as high fluorescence quantum yield, suitable pKa (5.1 in PBS) for biological applications, strong photostability, and acceptable biocompatibility. Motivated by this assumption that choosing the proper fluorophore may improve the selectivity toward $ONOO^-$, we incorporated a hydrazide group as a reactive site into BP613 to synthesize BP-ONOO (Scheme 1).

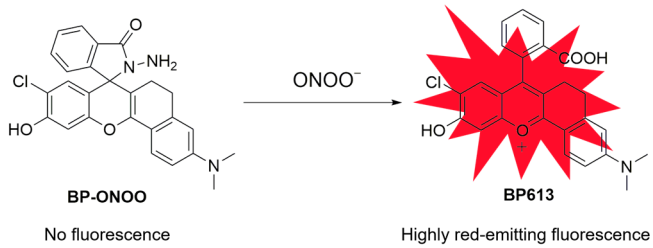

Scheme 1. Response mechanism of probe BP-ONOO to $ONOO^-$.

BP-ONOO exhibited numerous advantages for sensing $ONOO^-$ in biosystems, including: (1) a fluorescent turn-on signal change with a maximum excitation/emission at 570/613 nm; (2) excellent performance in aqueous solutions and physiological pH; (3) rapid response time (less than 4 s); (4) high sensitivity and low detection limit; and (5) remarkable selectivity toward other ROS/RNS and bio-relevant analytes. Furthermore, the probe demonstrated minimal cytotoxicity and enabled imaging of exogenous and endogenous $ONOO^-$ in RAW 264.7 macrophage cells.

2. Materials and Methods

2.1. Reagents and Instrumentation

All chemical reagents were purchased from commercial suppliers and used without further purification. ^1H and ^{13}C NMR spectra were obtained using a Bruker Advance 400 NMR spectrometer (internal standard: tetramethylsilane). Chemical shifts are expressed in ppm and coupling constants (*J*) are reported in hertz (Hz). High resolution mass spectra (HRMS) were collected on an AB SCIEX Triple TOF 5600+ mass spectrometer. UV-vis absorption spectra were obtained on a SHIMADZU UV-1800 spectrophotometer with

10 mm light path cuvette. Fluorescence spectra were recorded on a Hitachi F-4600 fluorescence spectrofluorometer (Kyoto, Japan). The absorbances for Cell Counting Kit-8 (CCK-8) analysis were recorded on a SpectraMax M5 Reader (Molecular Devices). Fluorescence images were recorded on an FV3000-IX83 confocal microscope (Olympus).

2.2. Synthesis of Compound **1**

Compound **1** (2-(5-chloro-2,4-dihydroxybenzoyl)benzoic acid) was synthesized according to the reported method [30]. 2′,7′-dichlorofluorescein-6-carboxylic acid (16.0 g, 40.0 mmol) was suspended in 160 mL of 50% aqueous NaOH (*w*/*v*) in a single neck flask and heated at 165 °C for 60 min under N_2 protection. The reaction was cooled down to room temperature and poured into 500 mL of ice water, acidified with concentrated HCl. The suspension was formed and filtered, the pale yellow solid **1** was dried under infrared lamp, and 9.6 g of the desired product (82% yield) was obtained. ^{1}H NMR (400 MHz, CD_3OD) δ 8.14 (dd, *J* = 7.8, 1.3 Hz, 1H), 7.74 (td, *J* = 7.5, 1.4 Hz, 1H), 7.67 (td, *J* = 7.6, 1.4 Hz, 1H), 7.40 (dd, *J* = 7.4, 1.3 Hz, 1H), 6.97 (s, 1H), 6.50 (s, 1H).

2.3. Synthesis of BP613

The synthetic route of BP613 is shown in Scheme S1. Compound **1** (876.0 mg, 3.0 mmol) and compound 2 (6-(dimethylamino)-3,4-dihydro-2H-naphthalen-1-one) (567.0 mg, 3.0 mmol) were dissolved in 60 mL methylsulfonic acid and heated at 110 °C overnight. The reaction solution was cooled down to room temperature and poured into 300 mL of ice water. The suspension was formed, then filtered. The crude product was subjected to silica gel chromatography with CH_2Cl_2/MeOH/TEA (20:1:1) as the eluent to obtain BP613 (776.0 mg, 58%) as a purple solid. ^{1}H NMR (400 MHz, CD_3OD + K_2CO_3) δ 8.08–8.03 (m, 1H), 7.93 (dd, *J* = 9.0, 1.2 Hz, 1H), 7.64–7.54 (m, 2H), 7.19–7.13 (m, 1H), 7.07 (s, 1H), 6.78–6.69 (m, 2H), 6.59–6.54 (m, 1H), 3.09 (s, 6H), 2.99–2.77 (m, 2H), 2.66 (ddd, *J* = 15.4, 8.9, 6.4 Hz, 1H), 2.49 (ddd, *J* = 15.3, 8.6, 6.2 Hz, 1H). ^{13}C NMR (100 MHz, CD_3OD + K_2CO_3) δ 174.9, 173.7, 163.1, 162.4, 158.6, 155.6, 145.4, 140.5, 134.9, 131.6, 131.1, 130.7, 130.3, 129.4, 128.7, 128.2, 118.3, 115.8, 115.4, 112.4, 111.5, 104.4, 40.2, 28.8, 25.1. HRMS (ESI): calculated for $C_{26}H_{21}ClNO_4^+$ [M^+] 446.1154, found 446.1154.

2.4. Synthesis of BP-ONOO

In a single neck flask, BP613 (223.0 mg, 0.5 mmol), EDCI (1-ethyl-(3-dimethylaminopro pyl)carbonyldiimide hydrochloride) (288.0 mg, 1.5 mmol), NHS (N-Hydroxy succinimide) (172.5 mg, 1.5 mmol), and a catalytic amount of DMAP (4-Dimethylaminopyridine) were dissolved in 5 mL DMF; the mixed solution was stirred under room temperature and monitored by TLC. After the starting material disappeared, the solvent was evaporated and the residue was purified by silica gel chromatography to get the intermediate product without further identification. Then, hydrazine hydrate (250 mg, 5 mmol) and the above intermediate product were dissolved in 5 mL DMF; the reaction mixture was stirred for another 4 h at 60 °C. The mixture was then extracted by ethyl acetate and water and the organic phase was concentrated in vacuo. The residue was subjected to silica gel chromatography with ethyl acetate/petroleum ether as eluent to afford BP-ONOO (131.0 mg, 57%) as a white solid. ^{1}H NMR (400 MHz, DMSO-d_6) δ 10.65 (s, 1H), 7.86–7.74 (m, 1H), 7.61–7.48 (m, 3H), 7.20 (d, *J* = 7.6 Hz, 1H), 6.87 (s, 1H), 6.64 (dd, *J* = 8.7, 2.5 Hz, 1H), 6.55 (d, *J* = 2.5 Hz, 1H), 6.35 (s, 1H), 4.60 (s, 2H), 2.93 (s, 6H), 2.76–2.67 (m, 1H), 2.54–2.43 (m, 1H), 1.87–1.79 (m, 1H), 1.45–1.37 (m, 1H). ^{13}C NMR (100 MHz, DMSO-d_6) δ 165.3, 153.4, 150.9, 150.5, 149.0, 146.0, 137.4, 132.6, 130.5, 128.8, 127.5, 123.3, 122.5, 122.3, 117.2, 115.3, 111.2, 111.0, 109.5, 103.7, 100.4, 65.7, 39.9, 27.9, 20.6. HRMS (ESI): calculated for $C_{26}H_{23}ClN_3O_3^+$ [M + H^+] 460.1422, found 460.1425.

2.5. Optical Detection Procedure for $ONOO^-$

Stock solution of 1 mM BP-ONOO was prepared in DMSO. Both absorbance and fluorescence measurements were performed in 20 mM PBS (pH = 7.4) and measured

in 1 cm light path quartz cuvettes. Excitation wavelength was 570 nm. The excitation and emission slits were 5 nm. Fluorescence titration studies: the concentration of BP-ONOO was fixed at 10 μM, and the final concentration of $ONOO^-$ was verified by adding different volumes of stock solution, BP-ONOO and $ONOO^-$ were mixed to a final volume of 400 μL, and the spectra were recorded after standing for 30 min at room temperature. The preparation methods of $ONOO^-$ and other ROS/RNS are described in the Supporting Information. Other stock solutions of interfering analytes were prepared in ultrapure water.

2.6. Cytotoxicity Assay of Probe

HeLa cells were cultured in RPMI-1640 medium containing 10% (*v*/*v*) fetal bovine serum (FBS) and 100 μg/mL penicillin-streptomycin in a humidified 37 °C, 5% CO_2 incubator. The cells were dispersed in a 96-well plate at a density of 5000 cells per well and maintained at the above condition for 24 h. Then, HeLa cells were incubated with various concentrations of BP-ONOO (0, 2, 5, 10, 15, and 20.0 μM) for 24 h; the media were then replaced with fresh media containing 10% CCK-8 and incubated for another 30 min. Then, the absorbance at 450 nm was measured, in which each concentration of BP-ONOO was performed three times.

2.7. Fluorescence Imaging Study for Endogenous and Exogenous $ONOO^-$

RAW 264.7 cells were cultured in Dulbecco's Modified Eagle Medium (DMEM) containing 10% (*v*/*v*) fetal bovine serum (FBS) and 100 μg/mL penicillin-streptomycin in a humidified 37 °C, 5% CO_2 incubator. Cells were seeded in glass-bottom dishes and incubated for one night before the imaging test.

For exogenous $ONOO^-$ detection, the adherent cells were rinsed three times with DMEM, pretreated with 10 μM BP-ONOO in culture media at 37 °C for 30 min, washed three times with DMEM, and incubated with various concentration of SIN-1 (0 μM, 20 μM, 50 μM, 100 μM, and 200 μM) for 30 min in serum-free DMEM at 37 °C. The cells were washed three times with PBS and the confocal imaging test was performed.

For endogenous $ONOO^-$ detection, the cells were stimulated with 1 μg/mL lipopolysa ccharide (LPS) and 1 μg/mL phorbol myristate acetate (PMA) for 6 h and 18 h respectively, washed three times using culture media, and incubated with 10 μM BP-ONOO in DMEM at 37 °C for 30 min. The cells were washed three times with PBS, then subjected to confocal imaging experiment. For the inhibition test, RAW 264.7 cells were treated with 1 μg/mL LPS and 1 μg/mL PMA in the presence of 200 μM minocycline, washed, and incubated with 10 μM BP-ONOO in DMEM in a sequential manner before their fluorescence images were finally acquired. For BP-ONOO, emission was collected at 600–700 nm (excited at 570 nm).

3. Results and Discussion

3.1. Synthesis of Probe

BP613 was prepared by reported method [29]. Subsequently, BP-ONOO was prepared via the condensation reaction between BP613 and hydrazine monohydrate using NHS and EDCI as condensation reagent (Scheme 2). Both BP613 and BP-ONOO was purified by silica gel column chromatography and confirmed by NMR and HRMS (Figures S1–S6).

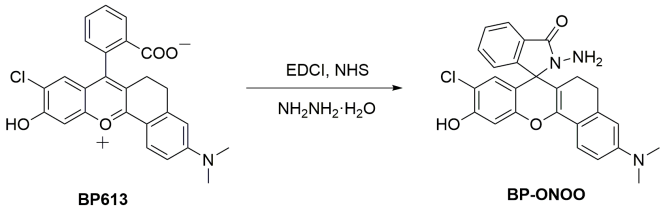

Scheme 2. Synthetic route for BP-ONOO.

3.2. Spectral Responses of BP-ONOO for ONOO⁻

Figure 1 shows the UV-vis absorption spectra and FL spectra of BP-ONOO before and after adding $ONOO^-$ in PBS (20 mM, pH = 7.4) at room temperature. The absorption spectrum of the free probe (10 μM) exhibits an ambiguous band in the visible region, rendering the solution colorless. Correspondingly, the fluorescence emission spectrum demonstrates an exceptionally low background with no discernible fluorescence signal. These observations can be attributed to the presence of a spirolactam structure in BP-ONOO, which disrupts the conjugated structure of the fluorophore [31]. Upon adding 40 μM $ONOO^-$, there is a noticeable change in solution color from colorless to purple, along with the appearance of an absorption band centered at 570 nm (Figure 1a). Simultaneously, a remarkable red-emitting fluorescence is observed with a significant enhancement peak at 613 nm (Figure 1b). These alterations indicate that BP-ONOO can serve as a red-emitting turn-on probe for $ONOO^-$.

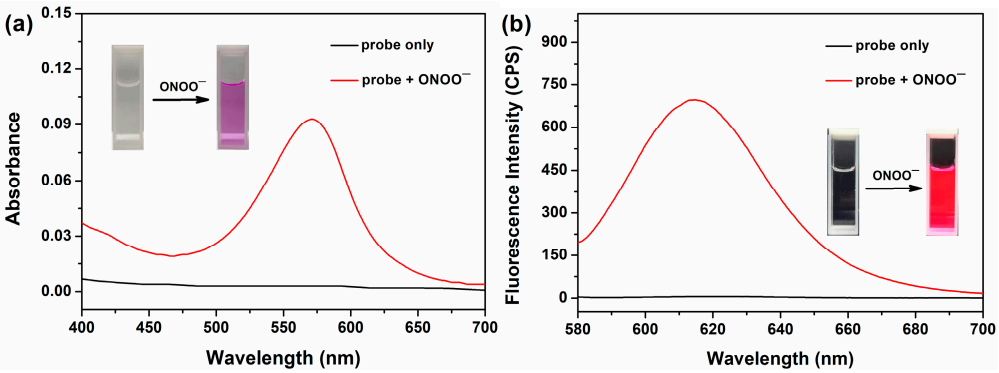

Figure 1. (**a**) UV-vis absorption and (**b**) fluorescence spectral changes of probe BP-ONOO (10 μM) before and after reacting with 40 μM $ONOO^-$ in PBS (20 mM, pH 7.4). The illustration in (**a**,**b**) shows (**a**) color change and (**b**) fluorescence change after addition of 40 μM $ONOO^-$. For fluorescent spectra: λ_{ex} = 570 nm, slit width: $d_{ex} = d_{em}$ = 5 nm.

The response of BP-ONOO to $ONOO^-$ exhibited remarkable rapidity, as demonstrated by the swift fluorescence enhancement reaching a plateau within 4 s (shown in Figure 2a). The characteristic confers significant advantages for real-time detection of transient $ONOO^-$ in living systems. We further investigated the influence of pH on the detection process. As shown in Figure 2b, the free probe solution (10 μM) exhibited negligible fluorescent signal variation when the pH ranged from 6 to 10, indicating its insensitivity to changes in pH. However, the addition of $ONOO^-$ resulted in a significant enhancement in fluorescence signal within the pH range of 7 to 9, indicating that the probe exhibits optimal performance under neutral and weak alkaline conditions.

The sensing mechanism of $ONOO^-$ was investigated by analyzing the high-resolution mass spectrometry of the reaction mixture containing BP-ONOO and equivalent $ONOO^-$. Figure S7 shows the emergence of a new mass peak at m/z = 446.1154, which corresponds to the calculated mass peak of BP613 (446.1154 for M^+), indicating the formation of BP613 during the reaction. Therefore, it can be reasonably speculated that the response mechanism is attributed to the activation of a carbonyl group in a spirolactam moiety, consistent with the design strategy employed for the well-known rhodamine-type fluorophores. The response mechanism is illustrated in Scheme 1, where non-fluorescent BP-ONOO reacts with $ONOO^-$ to generate BP613 and produce a fluorescence signal output.

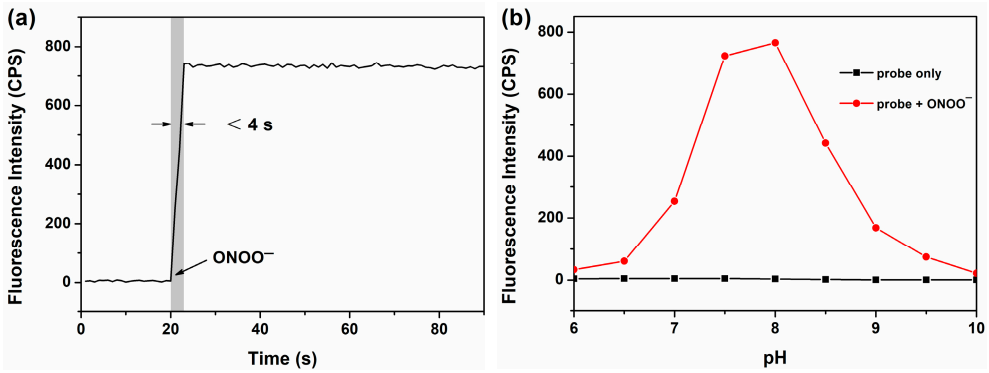

Figure 2. (**a**) Time course of the fluorescence intensity (613 nm) of BP-ONOO (10 μM) after addition of $ONOO^-$ (30 μM) in PBS (20 mM, pH 7.4) at 25 °C. (**b**) The effect of various pH values on fluorescence intensities at 613 nm of probe BP-ONOO (10 μM) in the absence and presence of $ONOO^-$ (30 μM) in PBS (20 mM). The data were recorded after standing for 30 s at room temperature. Λ_{ex} = 570 nm, λ_{em} = 613 nm, slit width: d_{ex} = d_{em} = 5 nm.

3.3. Quantitative Analysis of $ONOO^-$ Using BP-ONOO

The response of BP-ONOO towards $ONOO^-$ was subsequently evaluated through a fluorescence titration experiment. As shown in Figure 3a, the fluorescence intensity exhibited a gradual increase with the addition of increasing amounts of $ONOO^-$, reaching a plateau after approximately two equivalents of $ONOO^-$ were added. At saturation, the fluorescence intensity was enhanced up to 140-fold. The concentration–response curve is presented in Figure 3b, demonstrating that the fluorescence intensity enhancement at 613 nm displayed linearity with respect to the concentration of $ONOO^-$ within the range from 0 to 22.5 μM (linear equation: $y = 28.4983 \times [ONOO^-]$ (μM) + 4.9982, $R^2 = 0.9981$). The detection limit of BP-ONOO for $ONOO^-$ was estimated to be as low as 18 nM according to the 3σ criteria (defined as 3σ/slope, where σ is the standard deviation of blank solution), suggesting the high sensitivity for $ONOO^-$ detection. Hence, considering the relatively low concentration (nM–μM) of peroxynitrite in a complicated biological environment [13], we anticipate that BP-ONOO, exhibiting exceptional sensitivity, can serve as a potent tool for precise quantitative analysis of peroxynitrite within biological systems (Table S1).

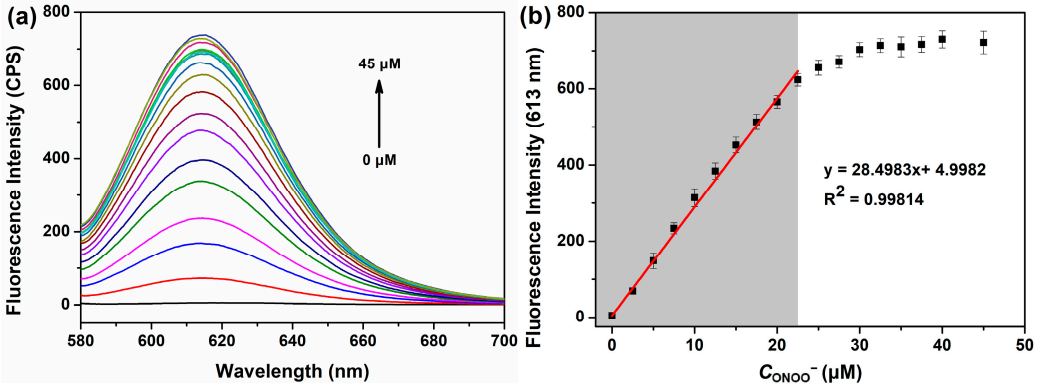

Figure 3. (**a**) Fluorescence spectra response of BP-ONOO (10 μM) toward different concentration of $ONOO^-$ (0–45 μM) in PBS (20 mM, pH = 7.4). (**b**) Fluorescence intensity (at 613 nm) changes of BP-ONOO under the varied concentration of $ONOO^-$ (0–45 μM). Fluorescence intensity (at 613 nm) and increased concentration of $ONOO^-$ from 0 to 22.5 μM was linearly fitted with the inserted equation. The spectrum was recorded after standing for 30 min at room temperature. Each measurement was performed in triplicate and the data are expressed as the mean ± SD. λ_{ex} = 570 nm, slit width: d_{ex} = d_{em} = 5 nm.

3.4. Selectivity of BP-ONOO

In order to assess the feasibility of the designed fluorescent probe in real sample analysis, various interferences were selected to investigate the selectivity of probe BP-ONOO, including reactive oxygen/nitrogen species (H_2O_2, ClO^-, $ROO^•$, TBHP, $^•NO$, $^•OH$, $O_2^{•-}$, and $ONOO^-$), common anions (S^{2-}, $S_2O_3^{2-}$, SO_3^{2-}, HSO_3^-, SCN^-, NO_2^-, F^-, Br^-, and I^-), metal ions (Ag^+, Ba^{2+}, Fe^{2+}, Fe^{3+}, Pb^{2+}, Zn^{2+}, Hg^{2+}, Mg^{2+}, Ni^{2+}, Ca^{2+}, Cu^{2+}, and Al^{3+}) as well as other biologically important substances (Vc, ATP, Lys, His, Glu, Gly, and GSH). As shown in Figure 4, the addition of 10 equivalents of interferences did not result in any significant fluorescence enhancement, which is highly promising. In contrast, the introduction of $ONOO^-$ led to a distinct increase in fluorescence intensity. These findings collectively demonstrate the excellent selectivity of BP-ONOO towards $ONOO^-$, thereby highlighting its highly desirable attributes as an effective probe.

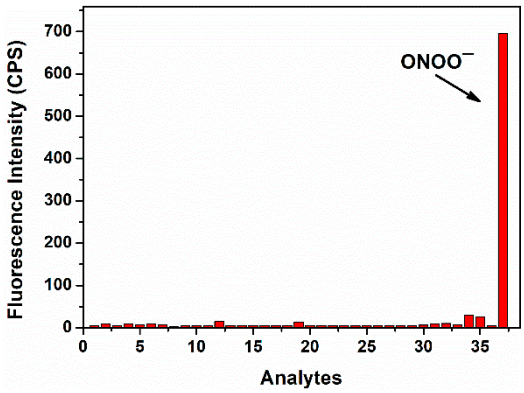

Figure 4. The fluorescence responses of probe BP-ONOO (10 μM) in the presence of various analytes (100 μM except for specific labels) in PBS (20 mM, pH = 7.4). 1. Blank, 2. Ag^+, 3. Ba^{2+}, 4. Fe^{2+}, 5. Fe^{3+}, 6. Pb^{2+}, 7. Zn^{2+}, 8. Hg^{2+}, 9. Mg^{2+}, 10. Ni^{2+}, 11. Ca^{2+}, 12. Cu^{2+}, 13. Al^{3+}, 14. S^{2-}, 15. $S_2O_3^{2-}$, 16. SO_3^{2-}, 17. HSO_3^-, 18. SCN^-, 19. NO_2^-, 20. F^-, 21. Br^-, 22. I^-, 23. Vc, 24. ATP, 25. Lys, 26. His, 27. Glu, 28. Gly, 29. GSH (1 mM), 30. H_2O_2, 31. ClO^-, 32. $ROO^•$, 33. TBHP, 34. $^•NO$, 35. $^•OH$, 36. $O_2^{•-}$, 37. $ONOO^-$ (30 μM). λ_{ex} = 570 nm, slit width: d_{ex} = d_{em} = 5 nm.

3.5. Cytotoxicity and Cell Imaging of BP-ONOO

Prior to the application of the fluorescence probe for exogenous and endogenous $ONOO^-$ imaging, we initially investigated the cytotoxicity of BP-ONOO. Figure 5 demonstrates that approximately 90% of the cells survived at a probe concentration of 20 μM, indicating the low cytotoxicity of BP-ONOO.

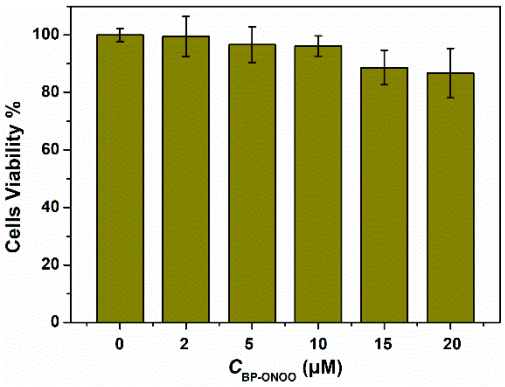

Figure 5. HeLa cell viability after treatment with different concentrations of BP-ONOO after 24 h; results of cytotoxicity assays were obtained via CCK-8 assay.

The capability of BP-ONOO to monitor exogenous and endogenous $ONOO^-$ was evaluated in live RAW 264.7 macrophage cells, which are recognized as model cells for generating ROS/RNS during inflammatory and immunological processes [32,33].

For imaging exogenous $ONOO^-$ (Figure 6), SIN-1 (3-morpholinosydnonimine hydrochloride, an $ONOO^-$ generator) was added at concentrations of 20 μM, 50 μM, 100 μM, and 200 μM. As shown in Figure 6(A2), no significant fluorescence was observed with only the probe BP-ONOO present. However, upon addition of SIN-1, a notable dose-dependent increase in fluorescence intensity was observed (B2–E2 in Figure 6). These results demonstrate that BP-ONOO can be utilized for imaging the external source of $ONOO^-$.

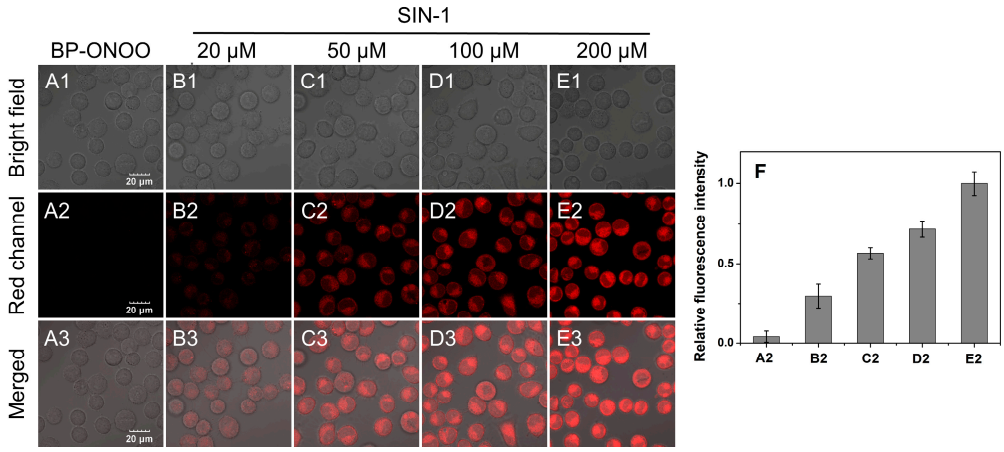

Figure 6. Confocal images of exogenous $ONOO^-$ at different concentrations in RAW 264.7 macrophage cells. Top: bright field images. Middle: fluorescence images. Bottom: merged images. (**A1**–**A3**) The cells were incubated with BP-ONOO (10 μM) for 30 min as control. The cells were incubated with BP-ONOO (10 μM) for 30 min followed by addition of (**B1**–**B3**) 20 μM, (**C1**–**C3**) 50 μM, (**D1**–**D3**) 100 μM, (**E1**–**E3**) 200 μM SIN-1 for another 30 min. Scale bar represents 20 μm. (**F**) Relative fluorescence intensity of fluorescence images from **A2** to **E2** (the fluorescence intensity from image E2 is defined as 1.0). The data are visualized by Image J software and expressed as mean ± SD (n = 3).

For endogenous $ONOO^-$ imaging, the cells were stimulated with lipopolysaccharide (LPS, 1 μg/mL) and phorbol myristate acetate (PMA, 1 μg/mL) for 6 h and 18 h respectively. Subsequently, the cells were incubated with BP-ONOO. As shown in Figure 7, a significant increase in intracellular fluorescence intensity (B2 and C2) was observed after treatment with LPS and PMA compared to the probe-only as control (A2). For the inhibition test, the RAW 264.7 cells were pre-treated with 1 μg/mL LPS and 1 μg/mL PMA in the presence of 200 μM minocycline (an $ONOO^-$ scavenger), followed by incubation with BP-ONOO for 30 min. Remarkably, there was a significant decrease in cellular fluorescence intensity observed (D2), providing compelling evidence that the probe effectively monitors endogenous $ONOO^-$ levels within living cells.

Finally, we investigated the sub-cellular distribution of BP-ONOO in HeLa cells. Commercially available LysoTracker Green, MitoTracker Green, and Hoechst 33342 were utilized to co-stain with BP-ONOO. As shown in Figure S8, after incubation with SIN-1 for 30 min, the fluorescence location of BP-ONOO was distributed throughout the cell. These results suggest that BP-ONOO can image $ONOO^-$ produced by various organelles and is mainly distributed in the cytoplasm.

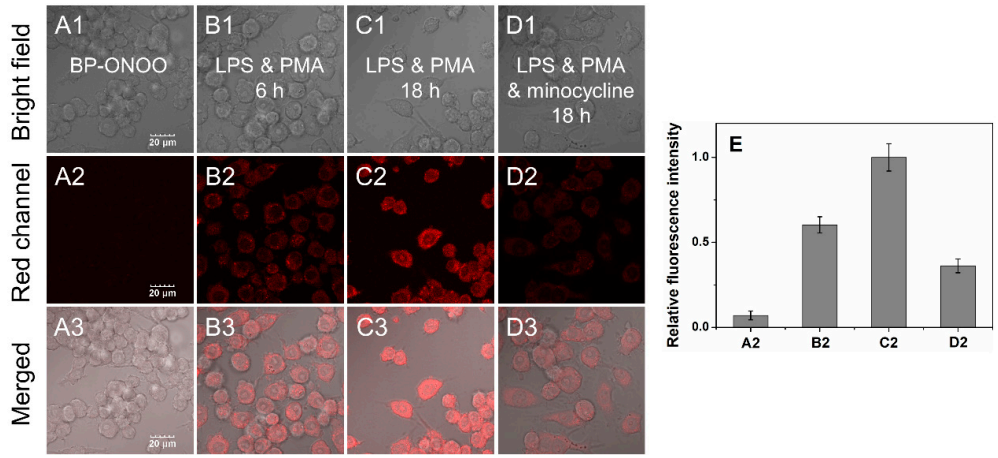

Figure 7. Confocal images of endogenous $ONOO^-$ in RAW 264.7 macrophage cells. Top: bright field images. Middle: fluorescence images. Bottom: merged images. (**A1**–**A3**) The cells were incubated with BP-ONOO (10 μM) for 30 min as control. (**B1**–**B3**) and (**C1**–**C3**) show the images that the cells were incubated with BP-ONOO (10 μM) for 30 min after pre-treatment with LPS (1 μg/mL) and PMA (1 μg/mL) for 6 h and 18 h respectively. (**D1**–**D3**) The cells were incubated with BP-ONOO (10 μM) for 30 min after pre-incubation with LPS (1 μg/mL), PMA (1 μg/mL), and minocycline (200 μM) for 18 h. Scale bar represents 20 μm. (**E**) Relative fluorescence intensity of fluorescence images from **A2** to **D2** (the fluorescence intensity from image **C2** is defined as 1.0). The data are visualized by Image J software and expressed as mean ± SD (n = 3).

4. Conclusions

In recent years, researchers have developed a variety of probes based on different recognition mechanism. However, some of these probes may encounter interference from higher concentrations of coexisting ROS/RNS in biological systems that undergo similar oxidation/nucleophilicity processes. Therefore, stringent requirements are imposed on the selectivity of these probes. Additionally, advancements have been made in long-wavelength/NIR probes, two-photon probes, and ratiometric probes. Among them, long wave-length/NIR probes have received great attention due to their excellent properties such as enhanced tissue penetration depth, reduced photodamage risk, and minimal interference from background fluorescence. Furthermore, given the chemical characteristics of $ONOO^-$, including low concentration (nM–μM) and short life (~ms) within complex biological environments, there remains an urgent need for the development of highly sensitive and rapid response probes.

In this work, we have developed a fluorescent probe, BP-ONOO, for monitoring $ONOO^-$ concentration levels. This probe consists of a rhodol-like red-emitting fluorophore with hydrazide as the recognition site. The BP-ONOO probe exhibits several advantageous properties including rapid response (<4 s), high sensitivity (LOD down to 18 nM), and excellent selectivity over other ROS/RNS and bio-relevant analytes. BP-ONOO demonstrates utilization for imaging endogenous/exogenous $ONOO^-$ in RAW 264.7 macrophage cells. Collectively, these compelling findings raise our expectations that BP-ONOO holds great promise as a valuable tool for unraveling the diverse roles and functions of $ONOO^-$ in living systems.

Supplementary Materials: The following supporting information can be downloaded at: https://www.mdpi.com/article/10.3390/chemosensors11110555/s1, Scheme S1: Synthetic route for BP613; Figure S1: ^1H NMR spectrum of probe BP613 in CD_3OD; Figure S2: ^{13}C NMR spectrum of probe BP613 in CD_3OD; Figure S3: ^1H NMR spectrum of probe BP-ONOO in $(CD_3)_2SO$; Figure S4: ^{13}C NMR spectrum of probe BP-ONOO in $(CD_3)_2SO$; Figure S5: HR-MS spectrum of probe BP613; Figure S6: HR-MS spectrum of probe BP-ONOO; Figure S7: Mass spectrum of BP-ONOO mixed with one equiv. of $ONOO^-$ in PBS buffer (20 mM, pH = 7.4); Figure S8: Co-localization experiment within HeLa cells. Cells were co-stained with BP-ONOO (20 μM) and commercial dyes sequentially, then treated

with SIN-1 (200 μM). Top: LysoTracker Green and BP-ONOO. Middle: MitoTracker Green and BP-ONOO. Bottom: Hoechst 33342 and BP-ONOO. (A1–C1) Bright field. (A2–C2) Channel of commercial dyes. (A3–C3) Channel of BP-ONOO. (A4–C4) Merged images of BP-ONOO and the corresponding dyes. (A5–C5) Fluores-cence intensity profiles of BP-ONOO and corresponding commercial dyes within the linear ROI. Scale bar represents 20 μm; Table S1: A comparison of fluorescent probes for $ONOO^-$ [34–42].

Author Contributions: Conceptualization, B.J. and X.L.; methodology, B.J., J.L. and X.L.; software, J.L.; validation, B.J., L.J. and W.L.; formal analysis, J.L. and X.L.; investigation, B.J., J.L., L.J. and W.L.; resources, B.J.; data curation, B.J., J.L., L.J. and W.L.; writing—original draft preparation, B.J.; writing—review and editing, B.J. and X.L.; visualization, J.L., L.J. and W.L.; project administration, B.J.; funding acquisition, B.J. All authors have read and agreed to the published version of the manuscript.

Funding: This research was funded by the National Natural Science Foundation of China (No. 21505075).

Institutional Review Board Statement: Not applicable.

Informed Consent Statement: Not applicable.

Data Availability Statement: Not applicable.

Conflicts of Interest: The authors declare no conflict of interest.

References

1. Goldstein, S.; Lind, J.; Merényi, G. Chemistry of Peroxynitrites as Compared to Peroxynitrates. *Chem. Rev.* **2005**, *105*, 2457–2470. [CrossRef] [PubMed]
2. Pryor, W.A.; Squadrito, G.L. The chemistry of peroxynitrite: A product from the reaction of nitric oxide with superoxide. *Am. J. Physiol.-Lung Cell. Mol. Physiol.* **1995**, *268*, L699–L722. [CrossRef] [PubMed]
3. Waris, G.; Ahsan, H. Reactive oxygen species: Role in the development of cancer and various chronic conditions. *J. Carcinog.* **2006**, *5*, 14. [CrossRef] [PubMed]
4. Ahmad, R.; Rasheed, Z.; Ahsan, H. Biochemical and cellular toxicology of peroxynitrite: Implications in cell death and autoimmune phenomenon. *Immunopharmacol. Immunotoxicol.* **2009**, *31*, 388–396. [CrossRef] [PubMed]
5. Szabo, C.; Ischiropoulos, H.; Radi, R. Peroxynitrite: Biochemistry, pathophysiology and development of therapeutics. *Nat. Rev. Drug Discov.* **2007**, *6*, 662–680. [CrossRef]
6. Ferrer-Sueta, G.; Campolo, N.; Trujillo, M.; Bartesaghi, S.; Carballal, S.; Romero, N.; Alvarez, B.; Radi, R. Biochemistry of Peroxynitrite and Protein Tyrosine Nitration. *Chem. Rev.* **2018**, *118*, 1338–1408. [CrossRef]
7. Finkel, T.; Serrano, M.; Blasco, M.A. The common biology of cancer and ageing. *Nature* **2007**, *448*, 767–774. [CrossRef]
8. Pacher, P.; Beckman, J.S.; Liaudet, L. Nitric oxide and peroxynitrite in health and disease. *Physiol. Rev.* **2007**, *87*, 315–424. [CrossRef]
9. Graham, P.M.; Li, J.Z.; Dou, X.; Zhu, H.; Misra, H.P.; Jia, Z.; Li, Y. Protection against peroxynitrite-induced DNA damage by mesalamine: Implications for anti-inflammation and anti-cancer activity. *Mol. Cell. Biochem.* **2013**, *378*, 291–298. [CrossRef]
10. Papaharalambus, C.A.; Griendling, K.K. Basic mechanisms of oxidative stress and reactive oxygen species in cardiovascular injury. *Trends Cardiovasc. Med.* **2007**, *17*, 48–54. [CrossRef]
11. Radi, R. Peroxynitrite, a stealthy biological oxidant. *J. Biol. Chem.* **2013**, *288*, 26464–26472. [CrossRef] [PubMed]
12. Wang, S.; Chen, L.; Jangili, P.; Sharma, A.; Li, W.; Hou, J.-T.; Qin, C.; Yoon, J.; Kim, J.S. Design and applications of fluorescent detectors for peroxynitrite. *Coord. Chem. Rev.* **2018**, *374*, 36–54. [CrossRef]
13. Sun, J.; Cao, X.; Lu, W.; Wei, Y.; Kong, L.; Chen, W.; Shao, X.; Wang, Y. Recent advances in fluorescent probes of peroxynitrite: Structural, strategies and biological applications. *Theranostics* **2023**, *13*, 1716–1744. [CrossRef]
14. Li, M.; Han, H.; Zhang, H.; Song, S.; Shuang, S.; Dong, C. Boronate based sensitive fluorescent probe for the detection of endogenous peroxynitrite in living cells. *Spectrochim. Acta A Mol. Biomol. Spectrosc.* **2020**, *243*, 118683. [CrossRef]
15. Xie, X.; Tang, F.; Liu, G.; Li, Y.; Su, X.; Jiao, X.; Wang, X.; Tang, B. Mitochondrial Peroxynitrite Mediation of Anthracycline-Induced Cardiotoxicity as Visualized by a Two-Photon Near-Infrared Fluorescent Probe. *Anal. Chem.* **2018**, *90*, 11629–11635. [CrossRef] [PubMed]
16. Wu, D.; Ryu, J.C.; Chung, Y.W.; Lee, D.; Ryu, J.H.; Yoon, J.H.; Yoon, J. A Far-Red-Emitting Fluorescence Probe for Sensitive and Selective Detection of Peroxynitrite in Live Cells and Tissues. *Anal. Chem.* **2017**, *89*, 10924–10931. [CrossRef]
17. Wu, Y.; Shi, A.; Li, Y.; Zeng, H.; Chen, X.; Wu, J.; Fan, X. A near-infrared xanthene fluorescence probe for monitoring peroxynitrite in living cells and mouse inflammation model. *Analyst* **2018**, *143*, 5512–5519. [CrossRef]
18. Jia, X.; Chen, Q.; Yang, Y.; Tang, Y.; Wang, R.; Xu, Y.; Zhu, W.; Qian, X. FRET-Based Mito-Specific Fluorescent Probe for Ratiometric Detection and Imaging of Endogenous Peroxynitrite: Dyad of Cy3 and Cy5. *J. Am. Chem. Soc.* **2016**, *138*, 10778–10781. [CrossRef]

19. Zhang, J.; Zhen, X.; Zeng, J.; Pu, K. A Dual-Modal Molecular Probe for Near-Infrared Fluorescence and Photoacoustic Imaging of Peroxynitrite. *Anal. Chem.* **2018**, *90*, 9301–9307. [CrossRef]
20. Yu, F.; Li, P.; Li, G.; Zhao, G.; Chu, T.; Han, K. A near-IR reversible fluorescent probe modulated by selenium for monitoring peroxynitrite and imaging in living cells. *J. Am. Chem. Soc.* **2011**, *133*, 11030–11033. [CrossRef]
21. Li, X.; Tao, R.R.; Hong, L.J.; Cheng, J.; Jiang, Q.; Lu, Y.M.; Liao, M.H.; Ye, W.F.; Lu, N.N.; Han, F.; et al. Visualizing peroxynitrite fluxes in endothelial cells reveals the dynamic progression of brain vascular injury. *J. Am. Chem. Soc.* **2015**, *137*, 12296–12303. [CrossRef]
22. Peng, T.; Chen, X.; Gao, L.; Zhang, T.; Wang, W.; Shen, J.; Yang, D. A rationally designed rhodamine-based fluorescent probe for molecular imaging of peroxynitrite in live cells and tissues. *Chem. Sci.* **2016**, *7*, 5407–5413. [CrossRef] [PubMed]
23. Sikora, A.; Zielonka, J.; Lopez, M.; Joseph, J.; Kalyanaraman, B. Direct oxidation of boronates by peroxynitrite: Mechanism and implications in fluorescence imaging of peroxynitrite. *Free Radic. Biol. Med.* **2009**, *47*, 1401–1407. [CrossRef] [PubMed]
24. Miao, J.; Huo, Y.; Liu, Q.; Li, Z.; Shi, H.; Shi, Y.; Guo, W. A new class of fast-response and highly selective fluorescent probes for visualizing peroxynitrite in live cells, subcellular organelles, and kidney tissue of diabetic rats. *Biomaterials* **2016**, *107*, 33–43. [CrossRef] [PubMed]
25. Cheng, D.; Peng, J.; Lv, Y.; Su, D.; Liu, D.; Chen, M.; Yuan, L.; Zhang, X. De Novo Design of Chemical Stability Near-Infrared Molecular Probes for High-Fidelity Hepatotoxicity Evaluation In Vivo. *J. Am. Chem. Soc.* **2019**, *141*, 6352–6361. [CrossRef]
26. Liu, D.; Feng, S.; Feng, G. A rapid responsive colorimetric and near-infrared fluorescent turn-on probe for imaging exogenous and endogenous peroxynitrite in living cells. *Sens. Actuators B Chem.* **2018**, *269*, 15–21. [CrossRef]
27. Zhu, B.; Zhang, M.; Wu, L.; Zhao, Z.; Liu, C.; Wang, Z.; Duan, Q.; Wang, Y.; Jia, P. A highly specific far-red fluorescent probe for imaging endogenous peroxynitrite in the mitochondria of living cells. *Sens. Actuators B Chem.* **2018**, *257*, 436–441. [CrossRef]
28. Zhang, R.; Zhao, J.; Han, G.; Liu, Z.; Liu, C.; Zhang, C.; Liu, B.; Jiang, C.; Liu, R.; Zhao, T.; et al. Real-Time Discrimination and Versatile Profiling of Spontaneous Reactive Oxygen Species in Living Organisms with a Single Fluorescent Probe. *J. Am. Chem. Soc.* **2016**, *138*, 3769–3778. [CrossRef]
29. Peng, R.; Yuan, J.; Cheng, D.; Ren, T.; Jin, F.; Yang, R.; Yuan, L.; Zhang, X. Evolving a Unique Red-Emitting Fluorophore with an Optically Tunable Hydroxy Group for Imaging Nitroreductase in Cells, in Tissues, and in Vivo. *Anal. Chem.* **2019**, *91*, 15974–15981. [CrossRef]
30. Xiong, X.; Song, F.; Chen, G.; Sun, W.; Wang, J.; Gao, P.; Zhang, Y.; Qiao, B.; Li, W.; Sun, S.; et al. Construction of long-wavelength fluorescein analogues and their application as fluorescent probes. *Chemistry* **2013**, *19*, 6538–6545. [CrossRef]
31. Kim, H.N.; Lee, M.H.; Kim, H.J.; Kim, J.S.; Yoon, J. A new trend in rhodamine-based chemosensors: Application of spirolactam ring-opening to sensing ions. *Chem. Soc. Rev.* **2008**, *37*, 1465–1472. [CrossRef] [PubMed]
32. Jacobs, A.T.; Ignarro, L.J. Lipopolysaccharide-induced Expression of Interferon-β Mediates the Timing of Inducible Nitric-oxide Synthase Induction in RAW 264.7 Macrophages*. *J. Biol. Chem.* **2001**, *276*, 47950–47957. [CrossRef] [PubMed]
33. Salonen, T.; Sareila, O.; Jalonen, U.; Kankaanranta, H.; Tuominen, R.; Moilanen, E. Inhibition of classical PKC isoenzymes downregulates STAT1 activation and iNOS expression in LPS-treated murine J774 macrophages. *Br. J. Pharmacol.* **2006**, *147*, 790–799. [CrossRef] [PubMed]
34. Uppu, R.M. Synthesis of peroxynitrite using isoamyl nitrite and hydrogen peroxide in a homogeneous solvent system. *Anal. Biochem.* **2006**, *354*, 165–168. [CrossRef]
35. Han, X.; Yang, X.; Zhang, Y.; Li, Z.; Cao, W.; Zhang, D.; Ye, Y. A novel activatable AIEgen fluorescent probe for peroxynitrite detection and its application in EC1 cells. *Sens. Actuators B Chem.* **2020**, *321*, 128510–128516. [CrossRef]
36. Zhang, J.; Li, Y.; Zhao, J.; Guo, W. An arylboronate-based fluorescent probe for selective and sensitive detection of peroxynitrite and its applications for fluorescence imaging in living cells. *Sens. Actuators B Chem.* **2016**, *237*, 67–74. [CrossRef]
37. Cheng, D.; Xu, W.; Yuan, L.; Zhang, X. Investigation of Drug-Induced Hepatotoxicity and Its Remediation Pathway with Reaction-Based Fluorescent Probes. *Anal. Chem.* **2017**, *89*, 7693–7700. [CrossRef]
38. Yang, R.; Dou, Y.; Zhang, Y.; Qu, L.; Sun, Y.; Li, Z. A facile and highly efficient fluorescent turn-on switch strategy based on diketone isomerization and its application in peroxynitrite fluorescent imaging. *Sens. Actuators B Chem.* **2021**, *337*, 129805–129813. [CrossRef]
39. Yu, F.; Li, P.; Wang, B.; Han, K. Reversible near-infrared fluorescent probe introducing tellurium to mimetic glutathione peroxidase for monitoring the redox cycles between peroxynitrite and glutathione in vivo. *J Am Chem Soc* **2013**, *135*, 7674–7680. [CrossRef]
40. Peng, T.; Wong, N.K.; Chen, X.; Chan, Y.K.; Sun, Z.; Hu, J.J.; Shen, J.; El-Nezami, H.; Yang, D. Molecular imaging of peroxynitrite with HKGreen-4 in live cells and tissues. *J. Am. Chem. Soc.* **2014**, *136*, 11728–11734. [CrossRef]
41. Li, H.; Li, X.; Wu, X.; Shi, W.; Ma, H. Observation of the Generation of $ONOO^-$ in Mitochondria under Various Stimuli with a Sensitive Fluorescence Probe. *Anal. Chem.* **2017**, *89*, 5519–5525. [CrossRef] [PubMed]
42. Li, J.; Peng, S.; Li, Z.; Zhao, F.; Han, X.; Liu, J.; Cao, W.; Ye, Y. Visualization of peroxynitrite in cyclophosphamide-induced oxidative stress by an activatable probe. *Talanta* **2022**, *238*, 123007–123013. [CrossRef] [PubMed]